

Compressive Isogeometric Analysis

Simone Brugiapaglia^{a,*}, Lorenzo Tamellini^b, Mattia Tani^b

^a*Department of Mathematics and Statistics, Concordia University. Montreal, Canada.*

^b*Consiglio Nazionale delle Ricerche, Istituto di Matematica Applicata e Tecnologie Informatiche “E. Magenes” (CNR-IMATI). Pavia, Italy.*

Abstract

This work is motivated by the difficulty in assembling the Galerkin matrix when solving Partial Differential Equations (PDEs) with Isogeometric Analysis (IGA) using B-splines of moderate-to-high polynomial degree. To mitigate this problem, we propose a novel methodology named COSSIGA (COMpreSSive ISOGeometric Analysis), which combines the IGA principle with CORSING, a recently introduced sparse recovery approach for PDEs based on compressive sensing. COSSIGA assembles only a small portion of a suitable IGA Petrov-Galerkin discretization and is effective whenever the PDE solution is sufficiently sparse or compressible, i.e., when most of its coefficients are zero or negligible. The sparsity of the solution is promoted by employing a multilevel dictionary of B-splines as opposed to a basis. Thanks to sparsity and the fact that only a fraction of the full discretization matrix is assembled, the proposed technique has the potential to lead to significant computational savings. We show the effectiveness of COSSIGA for the solution of the 2D and 3D Poisson equation over nontrivial geometries by means of an extensive numerical investigation.

Keywords: Isogeometric analysis, compressive sensing, sparse representations, hierarchical B-splines

1. Introduction

Isogeometric Analysis (IGA) is an alternative to standard Finite Element Analysis (FEA) that has attracted considerable attention by researchers in computational science and engineering communities since the seminal paper [23], published in 2005. IGA methodologies are quite similar to standard FEA, with the main difference that the basis functions used for representing the domain and the solution to the Partial Differential Equation (PDE) considered are splines rather than finite element basis functions. This apparently simple change generates many interesting features. These include the possibility of representing the geometry of the domain exactly, a more flexible choice of the polynomial degree and of the regularity of the basis used for approximating the solution, and a more effective error vs. degrees-of-freedom ratio than standard FEA. We refer the interested reader to [5] for a detailed mathematical analysis of the IGA method.

As all “young methods”, many aspects of IGA are still the subject of scientific investigation. The method proposed in this manuscript addresses one of these aspects, i.e. the fact that the assembly and resolution of IGA Galerkin linear systems is usually very expensive from the computational point of view, especially for moderate-to-high polynomial degrees of the spline basis functions. This aspect has been already tackled in several ways. Proposed approaches include switching from the usual element-based quadrature to a function-based quadrature [11, 31], more efficient matrix computation algorithms [3], low rank and sparse grids techniques [4, 21, 26], and efficient preconditioning [13, 14, 15, 22, 30, 32].

*Corresponding author

Email addresses: `simone.brugiapaglia@concordia.ca` (Simone Brugiapaglia), `tamellini@imati.cnr.it` (Lorenzo Tamellini), `mattia.tani@imati.cnr.it` (Mattia Tani)

In this paper, we propose instead a method in which the computational savings are potentially obtained by assembling only a small fraction of the full Galerkin matrix. The crucial underlying assumption is the sparsity (or compressibility) of the solution. Namely, if expanded with respect to a suitable basis, most of the solution coefficients should be zero (or negligible). Whether or not it is reasonable to expect such a feature in the solution to a PDE is therefore the first question that should be addressed. As will be clearer later, one notable example is the case of PDEs whose solutions exhibit multiscale features.

We mention in passing that another approach based on computing only a fraction of the Galerkin matrix has been recently proposed in [18]. However, in [18] the authors propose to compute a portion of the matrix exactly and then use this information to estimate the remaining entries of the matrix, so that, in the end, an approximation of the entire matrix is available. Instead, we propose to completely neglect some part of the matrix.

The method proposed in this paper is named COSSIGA (COmpreSSive IsoGeometric Analysis). This name refers to the fact that the method is an adaptation of the recently introduced CORSING (COmpressed SolvING) method [7, 9, 10] to the IGA framework. CORSING combines the Petrov-Galerkin method with compressive sensing [12, 16]. It assembles only a fraction of the discretization matrix and approximates the PDE solution via sparse recovery, using techniques such as ℓ^1 minimization or greedy algorithms. In this work, we extend the previous CORSING works, which were restricted to piecewise multilinear basis functions and rectangular domains, by using the IGA B-splines-based machinery to represent both the domain and the solution.

One notable difference with previous CORSING works is that here we do not use a hierarchical basis as set of trial functions (although this could be a viable approach given the well-established theory of hierarchical B-splines and their use in adaptive methods for PDEs - see [6] and references therein). In fact, we consider as trial functions a *dictionary* of splines obtained as a union of spline bases at different refinement levels (we use the term dictionary to refer to a generic, possibly redundant, system). The task of determining which splines should be activated is left to a sparse recovery algorithm. Thus, our approach can be seen as an alternative to standard adaptivity using hierarchical B-splines, where one does not need to implement any hierarchical basis, nor any marking/refining/derefining algorithms. Although redundant systems are widely employed in signal processing, their application in numerical analysis and scientific computing is a largely unexplored, yet very promising direction (see also [2]).

A first important disclaimer is that the goal of the manuscript is to show the potential of COSSIGA, but our implementation is not yet computationally effective. We actually prepared this initial manuscript with the idea of testing whether COSSIGA has *enough potential* to be worth implementing in a cost-effective way (which, by now, we believe it has). All numerical tests shown here have been implemented in GeoPDEs [33], available at <http://rafavzqz.github.io/geopdes/download/>. The fact that we do not have an efficient implementation of COSSIGA is the reason why in the numerical tests we do not discuss computational times and only show abstract indicators of computational cost such as the spline refinement level and the number of computed coefficients.

A second disclaimer is that upon completion of the manuscript we became aware of the work [24], which bears some similarities with COSSIGA. Our work shares with [24] the idea that using a spline dictionary instead of a basis could promote sparsity/compressibility of the PDE solution, and that a sparse version of the solution can then be recovered by suitable ℓ^1 minimization algorithms. However, in [24] randomized selection of the rows is not present and the compressive sensing paradigm is therefore not fully exploited. In fact, the entire Galerkin matrix is assembled, and not just a fraction of it as proposed here (in our opinion, this is where most of the computational gain can be potentially obtained). Furthermore, the numerical tests discussed in [24] only include 2D square domains, while here we take into account more general (2D and 3D) geometries. Finally, in [24] sparse recovery is performed via ℓ^1 minimization, whereas we employ the greedy algorithm orthogonal matching pursuit.

The rest of this paper is organized as follows. The methodology is explained in Section 2. In particular, a brief recap on the basics of IGA is given in Section 2.2, and the construction of the multilevel spline dictionary is detailed in Section 2.3. The Petrov-Galerkin formulation, which is the proper formal setting of the COSSIGA method, is introduced in Section 2.4. Finally, the two Sections

2.5 and 2.6 give a detailed explanation of the specifics of CossIGA (the approach is summarized in Algorithm 2.1). An extensive numerical investigation is then carried out in Section 3: in particular, we consider two test cases in 2D and one in 3D; a test comparing the effectiveness of C^0 vs. C^{p-1} splines (p being their polynomial degree) is also provided. Finally, Section 4 gathers conclusive remarks and future work directions.

2. The CossIGA method

2.1. Problem setting

Let us consider the weak formulation of the homogeneous Poisson equation over a domain $\Omega \subseteq \mathbb{R}^d$, with $d = 2, 3$

$$\text{find } u \in H_0^1(\Omega) : \quad a(u, v) = \int_{\Omega} f(\mathbf{x})v(\mathbf{x})d\mathbf{x}, \quad \forall v \in H_0^1(\Omega), \quad (1)$$

where $a(\cdot, \cdot) : H_0^1(\Omega) \times H_0^1(\Omega) \rightarrow \mathbb{R}$ is the bilinear form defined by

$$a(u, v) = \int_{\Omega} \nabla u(\mathbf{x}) \cdot \nabla v(\mathbf{x})d\mathbf{x}, \quad (2)$$

and where $f \in H^{-1}(\Omega)$ is a forcing term. The method can be easily generalized to more general weak problems in Hilbert spaces, such as advection-diffusion-reaction equations.

In this section we will formally introduce all the technical elements needed to define the CossIGA approach. The main ideas employed are based on the CORSING method [10, 9]. In short, we will consider a Petrov-Galerkin discretization of (1), where the test space is randomly subsampled according to the so-called local a -coherence and sparse recovery of an approximate solution to (1) is performed via Orthogonal Matching Pursuit (OMP).

2.2. B-splines and the Isogeometric Analysis principle

Given two natural numbers $n, p \in \mathbb{N}$, we define the *knot vector* over the unit interval $\hat{I} := [0, 1]$ as $\Xi = [\xi_1, \xi_2, \dots, \xi_{n+p+1}]$ with nondecreasing and possibly repeated entries, such that $\xi_1 = 0$ and $\xi_{n+p+1} = 1$. Each ξ_i is a *knot* and any interval (ξ_i, ξ_{i+1}) having nonzero length is an *element*. Let us further denote the total number of elements as N_{el} . In this paper, the elements will have the same length, called *mesh size* and denoted by h . Moreover, we assume the knot vector Ξ to be *open*, i.e. we let its first and last knots have multiplicity $p+1$ (i.e., they are repeated $p+1$ times). Observe that also internal knots could have multiplicity greater than one. Finally, we define the nondecreasing vector $Z = [\zeta_1, \dots, \zeta_{N_{\text{el}}+1}]$ as the vector of knots of Ξ without repetitions, and let m_i be the multiplicity of ζ_i in Ξ , so that $\sum_{i=1}^{N_{\text{el}}+1} m_i = n + p + 1$.

Given the knot vector Ξ thus built, we define the B-splines by means of the Cox-De Boor recursive formula. We start with piecewise constant splines

$$\hat{B}_{i,0}(\xi) = \begin{cases} 1, & \xi_i \leq \xi < \xi_{i+1}, \\ 0, & \text{otherwise,} \end{cases} \quad \text{for } i = 1, \dots, n+p.$$

Then, for $\bar{p} = 1, \dots, p$, we have the recursive step

$$\hat{B}_{i,\bar{p}}(\xi) = \begin{cases} \frac{\xi - \xi_i}{\xi_{i+\bar{p}} - \xi_i} \hat{B}_{i,\bar{p}-1}(\xi) + \frac{\xi_{i+\bar{p}+1} - \xi}{\xi_{i+\bar{p}+1} - \xi_{i+1}} \hat{B}_{i+1,\bar{p}-1}(\xi), & \xi_i \leq \xi < \xi_{i+\bar{p}+1}, \\ 0, & \text{otherwise,} \end{cases} \quad \text{for } i = 1, \dots, n+p-\bar{p},$$

with the convention that $0/0 = 0$. Note that if the knot vector Ξ is open, the corresponding basis is interpolatory in the first and last knots. The B-splines just defined form a basis for the space $S_p(\Xi, \hat{I})$ of spline-polynomials, i.e., of piecewise polynomials of degree p and regularity C^{p-m_i} at ζ_i ,

$$S_p(\Xi, \hat{I}) = \text{span}\{\hat{B}_{i,p} : i = 1, \dots, n\}.$$

In particular, the maximal regularity of a spline at the knots is C^{p-1} . In the following, we will be interested in the cases where all the internal knots of Ξ_l are either repeated once or $p-1$ times: in the former case, we talk about spline of maximal regularity or C^{p-1} splines, while in the latter we talk about C^0 splines. Moreover, since we are considering homogeneous boundary conditions, we consider the set of B-splines that vanish at the boundary:

$$S_p^{\text{int}}(\Xi, \hat{I}) = \text{span}\{\hat{B}_{i,p} : i = 2, \dots, n-1\}.$$

For $d = 2$ we define the parametric domain $\hat{\Omega} = \hat{I} \times \hat{I}$ (extension to the case $d > 2$ is analogous). We consider two open knot vectors Ξ_1, Ξ_2 with $n_1 + p_1 + 1$ and $n_2 + p_2 + 1$ knots respectively, the corresponding knots without repetitions Z_1, Z_2 , and the tensor products $\Xi = \Xi_1 \times \Xi_2$, $Z = Z_1 \times Z_2$; in particular, Z generates a cartesian mesh over $\hat{\Omega}$ composed of $N_{\text{el},1} N_{\text{el},2}$ rectangular elements. Taking tensor products of the univariate B-splines over Ξ_1 and Ξ_2 we obtain a basis for the space of bivariate spline polynomials and the corresponding basis of B-splines satisfying homogeneous boundary conditions. To this end, we introduce the multi-indices $\mathbf{i} = (i_1, i_2), \mathbf{p} = (p_1, p_2)$ and let $\hat{B}_{\mathbf{i},\mathbf{p}}(\xi_1, \xi_2) = \hat{B}_{i_1,p_1}(\xi_1)\hat{B}_{i_2,p_2}(\xi_2)$, so that

$$\begin{aligned} S_{\mathbf{p}}(\Xi, \hat{\Omega}) &= \text{span}\{\hat{B}_{\mathbf{i},\mathbf{p}} : 1 \leq i_1 \leq n_1, 1 \leq i_2 \leq n_2\}, \\ S_{\mathbf{p}}^{\text{int}}(\Xi, \hat{\Omega}) &= \text{span}\{\hat{B}_{\mathbf{i},\mathbf{p}} : 2 \leq i_1 \leq n_1 - 1, 2 \leq i_2 \leq n_2 - 1\}. \end{aligned}$$

In the following, we will assume that $p_1 = p_2 = p$, so that we can drop the bold notation \mathbf{p} and write p instead. Moreover, we enumerate the B-splines with a single index i ranging from 1 to $n = n_1 n_2$ for $S_p(\Xi, \hat{\Omega})$, and from 1 to $n^{\text{int}} = (n_1 - 1)(n_2 - 1)$ for $S_p^{\text{int}}(\Xi, \hat{\Omega})$, i.e.,

$$S_p(\Xi, \hat{\Omega}) = \text{span}\{\hat{B}_{i,p} : 1 \leq i \leq n\}, \quad S_p^{\text{int}}(\Xi, \hat{\Omega}) = \text{span}\{\hat{B}_{i,p} : 1 \leq i \leq n^{\text{int}}\}.$$

We assume that the computational domain Ω can be parameterized by a mapping $F : \hat{\Omega} \rightarrow \Omega$, obtained as a linear combination of B-splines with given control points $\mathbf{P}_1, \dots, \mathbf{P}_n \in \mathbb{R}^2$, i.e.,

$$\mathbf{x} \in \Omega \iff \mathbf{x} = F(\boldsymbol{\xi}) = \sum_{1 \leq i \leq n} \hat{B}_{i,p}(\boldsymbol{\xi}) \mathbf{P}_i, \quad \text{for some } \boldsymbol{\xi} \in \hat{\Omega}.$$

We mention in passing that many geometries Ω of practical interest, such as circles and ellipses, cannot be represented exactly by B-splines. However, *nonuniform rational B-splines* (NURBS) can be employed for this purpose (see [5, 23] for details). As the name suggests, NURBS are ratios of B-splines and retain most of the properties of B-splines, so in the rest of this manuscript we use “splines” as a comprehensive term for both B-splines and NURBS.

According to the IGA principle, splines are also employed to approximate the solution u to the weak problem (1). To this end, we introduce the splines on the physical domain, defined by

$$B_{i,p} := \hat{B}_{i,p} \circ F^{-1},$$

and the spline space on the physical domain Ω as follows:

$$S_p(\Xi, \Omega) = \text{span}\{B_{i,p} : 1 \leq i \leq n\}, \quad S_p^{\text{int}}(\Xi, \Omega) = \text{span}\{B_{i,p} : 1 \leq i \leq n^{\text{int}}\}.$$

Finally, we define a basis of $S_p^{\text{int}}(\Xi, \Omega)$ normalized with respect to the $H^1(\Omega)$ -seminorm as follows:

$$\mathcal{B}_p^{\text{int}}(\Xi, \Omega) = \left\{ \frac{B_{i,p}}{|B_{i,p}|_{H^1(\Omega)}} : 1 \leq i \leq n^{\text{int}} \right\}.$$

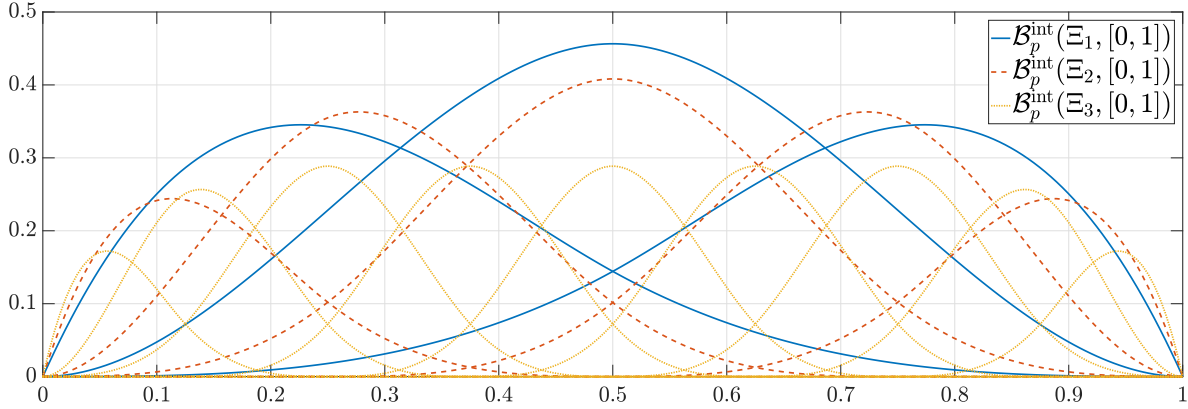


Figure 1: The dictionary $\Psi_{p,l_0,L}$, for $p = 3, l_0 = 1, L = 3$, and splines of regularity C^2 .

2.3. Multilevel dictionary of B-splines and the sparsity assumption

To apply the compressive sensing principle, we need to generate a sparse (or compressible) representation of the solution u to (1). Namely, we need to identify a basis or, more in general, a dictionary such that most of the coefficients of the corresponding expansion of u are zero (or negligible). With this aim, we resort to a multiscale decomposition that is able to enhance compressibility in solutions with, e.g., local features or sharp transitions. Given $l_0, L \in \mathbb{N}$ such that $1 \leq l_0 < L$, we consider the multilevel dictionary of B-splines

$$\Psi_{p,l_0,L} := \bigcup_{l=l_0}^L \mathcal{B}_p^{\text{int}}(\Xi_l, \Omega) = \{\psi_j\}_{j \in [N_{\text{dict}}]}, \quad (3)$$

where $\Xi_{l_0} \subseteq \dots \subseteq \Xi_L$ is a nested sequence of knot vectors such that Ξ_l corresponds to a grid of meshsize $h_l = 2^{-l}$ associated with B-splines of degree p and where we adopted the notation $[k] = \{1, \dots, k\}$, for every $k \in \mathbb{N}$. The dictionary $\{\psi_j\}_{j \in [N_{\text{dict}}]}$ is assumed to be ordered lexicographically with respect to the multi-index (l, i) : the level l and the index i of each (normalized) spline $B_{i,p}$ in $\mathcal{B}_p^{\text{int}}(\Xi_l, \Omega)$. A plot of the dictionary $\Psi_{3,1,3}$ is shown in Figure 1. The intuition is the following: all (or most of) the splines in the lowest levels are activated to approximate the coarse component of the solution and only a few splines in the high-resolution levels are activated to capture local features or sharp transitions. The dictionary $\Psi_{p,l_0,L}$ has been also considered in [24].

In standard hierarchical approaches, only a linearly independent subset of $\Psi_{p,l_0,L}$ is selected. This is typically done by starting from the coarsest basis, then marking a region where the error is concentrated, refining in that region while preserving linear independence, and repeating this process until the solution is accurate enough. Instead, in our approach the splines in the dictionary to be activated are identified by solving a particular minimization problem, as we will discuss in the following. However, before doing this, we need to make a short digression about the cardinality and the number of degrees of freedom (i.e., the dimension of the span) of the dictionary $\Psi_{p,l_0,L}$.

In our numerical tests (Section 3) we will use either C^{p-1} splines or C^0 splines. Hence, we recall explicit formulas for the cardinality of $\mathcal{B}_p^{\text{int}}(\Xi_l, \Omega)$ in these two cases:

$$|\mathcal{B}_p^{\text{int}}(\Xi_l, \Omega)| = \begin{cases} 2^l + p - 2, & \text{for } C^{p-1} \text{ splines,} \\ 2^l p - 1, & \text{for } C^0 \text{ splines.} \end{cases} \quad (4)$$

Clearly, the cardinality of the dictionary is

$$N_{\text{dict}} = |\Psi_{p,l_0,L}| = \sum_{l=l_0}^L |\mathcal{B}_p^{\text{int}}(\Xi_l, \Omega)|. \quad (5)$$

Notice that the span of the last hierarchical level coincides with the span of the whole dictionary, due to the fact that B-splines in $\mathcal{B}_p^{\text{int}}(\Xi_l, \Omega)$ are linear combinations of B-splines in $\mathcal{B}_p^{\text{int}}(\Xi_L, \Omega)$, for every $l \leq L$. Namely,

$$\text{span}(\Psi_{p,l_0,L}) = S_p^{\text{int}}(\Xi_L, \Omega). \quad (6)$$

Therefore, combining (4) and (6), the number of degrees of freedom (dof) of the dictionary $\Psi_{p,l_0,L}$ coincides with the cardinality of the basis at level L , i.e.,

$$N_{\text{dof}} = \begin{cases} (2^L + p - 2)^d & \text{for } C^{p-1} \text{ splines,} \\ (2^L p - 1)^d & \text{for } C^0 \text{ splines.} \end{cases} \quad (7)$$

The size of the dictionary is in general comparable to the size of the basis at level L . In fact, it is not difficult to show that, for any d and p , $N_{\text{dict}} \leq 3N_{\text{dof}}$ for C^{p-1} splines (for L large enough) and $N_{\text{dict}} \leq 2N_{\text{dof}}$ for C^0 splines (for any L).¹

We can now come back to the main topic of introducing the minimization approach to select the B-splines from the dictionary to be used to represent the solution u . As already said, we considered a multilevel dictionary hoping that only a few B-splines will be needed in order to well approximate u : most of those in the lowest levels (which are not many) will be used to approximate the coarse component of the solution and only a few splines in the higher levels will be used to capture local features or sharp transitions. In other words, we aim at computing a sparse approximation \tilde{u} to u , i.e., a function of the form

$$\tilde{u} = \sum_{j=1}^{N_{\text{dict}}} \tilde{u}_j \psi_j, \quad \text{with } \|\tilde{\mathbf{u}}\|_0 \ll N_{\text{dict}}, \quad (8)$$

where, for every $\mathbf{v} \in \mathbb{R}^k$, $\|\mathbf{v}\|_0 := |\{v_j \neq 0\}|$. More specifically, we say that \tilde{u} is s -sparse if $\|\tilde{\mathbf{u}}\|_0 \leq s$. Given a budget of s coefficients, the goal is to compute an s -sparse approximation such that $\|u - \tilde{u}\|_{H^1(\Omega)}$ is as close as possible to the best s -term approximation error of u with respect to $\Psi_{p,l_0,L}$, defined by

$$\sigma_s(u)_{H^1(\Omega)} = \inf_{\|\mathbf{z}\|_0 \leq s} \left\| u - \sum_{j \in [N_{\text{dict}}]} z_j \psi_j \right\|_{H^1(\Omega)}. \quad (9)$$

If $\sigma_s(u)_{H^1(\Omega)}$ has a fast decay with respect to s (e.g., $\sigma_s(u)_{H^1(\Omega)} \leq Cs^{-\alpha}$ for some $C, \alpha > 0$), u is informally said to be *compressible* with respect to $\Psi_{p,l_0,L}$.

2.4. Petrov-Galerkin: B-splines vs. sine functions

Together with the sparsity-promoting dictionary just introduced, we consider a Petrov-Galerkin (PG) discretization of (1). We use the functions in the dictionary $\Psi_{p,l_0,L}$ as trial functions of the PG formulation, i.e. we approximate u as a linear combination of functions in $\Psi_{p,l_0,L}$. We choose the test functions according to a principle that lies at the core of compressive sensing and also employed in CORSING. Namely, since the trial functions are localized in the space domain, it is convenient to choose test functions localized in the frequency (or Fourier) domain. The underlying intuition is that functions that are sparse in the space domain cannot be too sparse in the frequency domain (this is the so-called uncertainty principle [17]). In our setting, we employ test functions of Fourier type to measure the solution in the frequency domain. Now, thanks to sparsity the amount of information

¹For C^{p-1} splines,

$$N_{\text{dict}} = N_{\text{dof}} + \sum_{l=l_0}^{L-1} (2^l + p - 2)^d \leq N_{\text{dof}} + \left(\sum_{l=l_0}^{L-1} (2^l + p - 2) \right)^d = N_{\text{dof}} + \left(2^L - 2^{l_0} + (L - l_0)(p - 2) \right)^d.$$

Therefore, if $p \geq 2$ and L is large enough to have $(L - l_0 - 2^{1/d})(p - 2) \leq 2^L(2^{1/d} - 1) + 2^{l_0}$, we obtain $N_{\text{dict}} \leq 3N_{\text{dof}}$. The computation is similar for $p = 1$ or for C^0 splines.

intrinsically needed to represent the solution is very small; yet, the information in the frequency domain is spread over the whole spectrum due to the uncertainty principle. Therefore, Fourier measurements of signals that are sparse in space are highly redundant. In order to get rid of this redundancy, the idea of compressive sensing is to select only a few of them in a randomized way.

For this reason, we consider the sine functions over \widehat{I}^d , defined by

$$\sin_{\mathbf{r}}(\boldsymbol{\xi}) := \prod_{i=1}^d \sin(r_i \pi \xi_i), \quad \forall \boldsymbol{\xi} \in \widehat{I}^d, \forall \mathbf{r} \in \mathbb{N}^d. \quad (10)$$

Given a maximum frequency $R \in \mathbb{N}$, the corresponding basis of test functions defined over $\widehat{\Omega}$ is

$$\Phi_R := \left\{ \frac{\sin_{\mathbf{r}} \circ F^{-1}}{|\sin_{\mathbf{r}} \circ F^{-1}|_{H^1(\Omega)}} : \mathbf{r} \in [R]^d \right\} = \{\varphi_q\}_{q \in [N_{\text{test}}]}, \quad (11)$$

where the definition of the set $\{\varphi_q\}_{q \in [N_{\text{test}}]}$ implicitly depends on the ordering used over the multi-index set $[R]^d$ (e.g., the lexicographic ordering) and where $|\Phi_R| =: N_{\text{test}} = R^d$. The resulting PG discretization of (1) with respect to the trial and test functions in $\Psi_{p,l_0,L}$ and Φ_R , respectively, is

$$B\mathbf{z} = \mathbf{c}, \quad (12)$$

where $B \in \mathbb{R}^{N_{\text{test}} \times N_{\text{dict}}}$ and $\mathbf{c} \in \mathbb{R}^{N_{\text{test}}}$ are defined as

$$B_{qj} := a(\psi_j, \varphi_q), \quad c_q := \int_{\Omega} f \varphi_q, \quad \forall j \in [N_{\text{dict}}], \forall q \in [N_{\text{test}}]. \quad (13)$$

A sufficient requirement to have a well-posed PG formulation is the following discrete inf-sup condition (see, e.g., [28, Theorem 5.3.1]):

$$\inf_{u \in \text{span}(\Psi_{p,l_0,L})} \sup_{v \in \text{span}(\Phi_R)} \frac{a(u, v)}{\|u\|_{H^1(\Omega)} \|v\|_{H^1(\Omega)}} \geq \alpha > 0. \quad (14)$$

Note that (14) is a condition on the vector spaces spanned by the trial and the test functions. A necessary condition to have $\alpha > 0$ is

$$N_{\text{test}} \geq N_{\text{dof}}. \quad (15)$$

Moreover, α is nondecreasing with respect to R or, equivalently, to N_{test} . In practice, in view of (4), we make the heuristic choice

$$R = \begin{cases} 1.5 \lceil 2^L + p - 2 \rceil & \text{for } C^{p-1} \text{ splines,} \\ 1.5 \lceil 2^L \times p - 1 \rceil & \text{for } C^0 \text{ splines.} \end{cases} \quad (16)$$

where $\lceil x \rceil$ rounds a real number x to the closest integer greater than or equal to x . The factor 1.5 in Equation (16), which in particular implies condition (15), has been empirically chosen based on numerical experimentation. Studying the relation between α and R from the theoretical standpoint is an open problem. Some theoretical insights on this issue are given by the so-called restricted inf-sup property analysis, introduced in [10].

Since we are assuming u to be well approximated by a sparse function \tilde{u} of the form (8), we look for an s -sparse approximate solution to (12), obtained by solving

$$\min_{\mathbf{z} \in \mathbb{R}^{N_{\text{dict}}}} \|B\mathbf{z} - \mathbf{c}\|_2 \quad \text{s.t.} \quad \|\mathbf{z}\|_0 \leq s, \quad (17)$$

for a suitable small value of $s \in \mathbb{N}$ (such that $s \ll N_{\text{dofs}} \leq N_{\text{dict}}$) chosen by the user. This problem is actually NP-hard [27] but it can be approximately solved by sparse recovery approaches such as Orthogonal Matching Pursuit (OMP) (see, e.g., [19, Section 3.2]). Of course, OMP is not the only

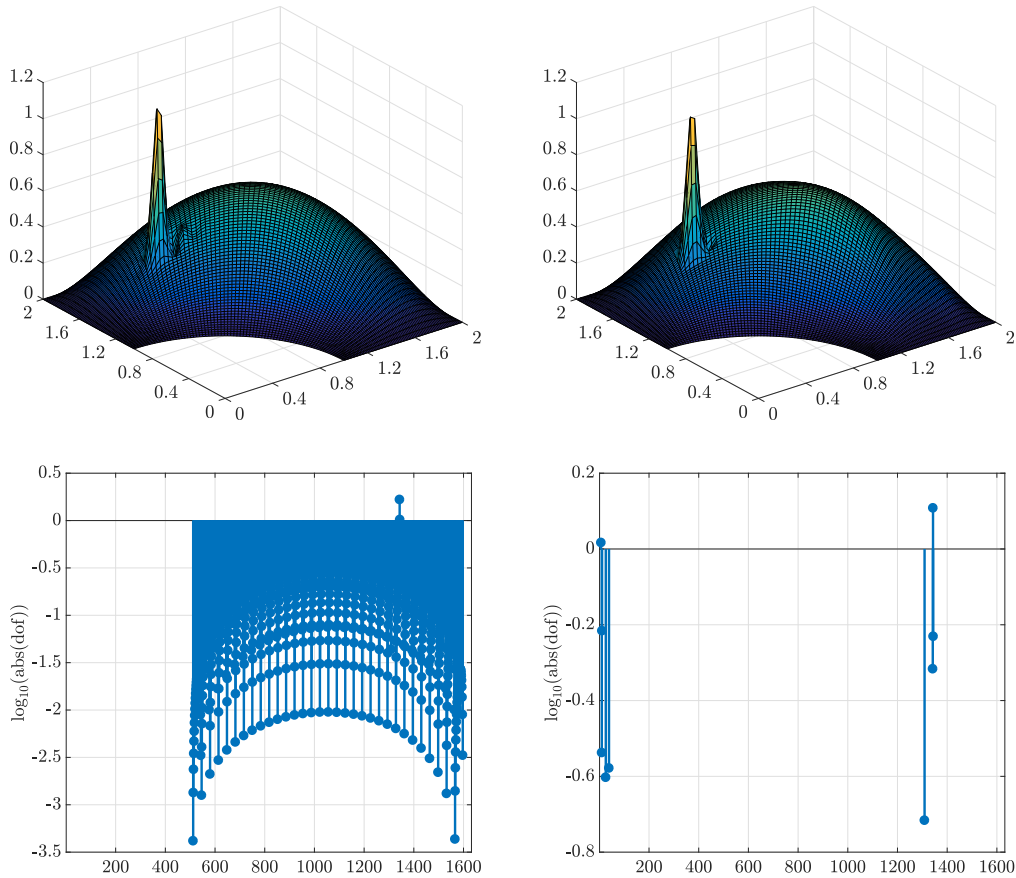


Figure 2: Left: standard IGA-Galerkin solution to the problem discussed in Section 3.2 (i.e., the solution computed by solving the square linear system obtained using as trial and test functions the B-splines at the finest discretization level Ξ_L); Right: its approximation computed using OMP to solve the PG system (12) in the sense of equation (17); here we have enforced OMP to compute $s = 9$ coefficients. The top row shows the computed solutions with both approaches and the bottom row shows the size of the coefficients in log scale (so-called “stem plots”). The horizontal axis in both stem plots shows the lexicographically-ordered indices of the B-splines in the dictionary $\Psi_{p,l_0,L}$ with $p = 2, l_0 = 1, L = 5$ ($N_{\text{dict}} = 1632$ and $N_{\text{dof}} = 1024$), with the understanding that the IGA-Galerkin solution only uses the basis at level $L = 5$, i.e., the last of the bases that compose the dictionary $\Psi_{p,l_0,L}$ (this is why the IGA stem plot is shifted rightward). For the standard IGA-Galerkin, we need to activate all the coefficients; conversely, the redundancy of the spline dictionary significantly promotes sparsity, so that we only need $s = 9$ coefficients to recover a decent approximation of the solution by solving the PG system with OMP: 5 for the coarse part of the solution and 4 for the localized feature.

option to compute sparse solutions to (12). Other choices include ℓ^1 minimization and thresholding algorithms (see [19, Section 3]). In this context, we choose OMP thanks to its ability to easily control the number of iterations given an estimate s of the sparsity level and its computational efficiency for small values of s (see [9, Section 5] for a numerical comparison between ℓ^1 minimization and OMP for sparse numerical approximation of PDEs). As an example, Figure 2 clearly shows the effectiveness of using a multilevel dictionary in a PG setting and then resorting to OMP to compute a sparse approximate solution to the corresponding linear system.

2.5. CossIGA

The final step is to reduce the dimensionality of the linear system (12) via randomized subsampling. In other words, we aim at computing a sparse approximation \tilde{u} to u of the form (8) without assembling the full PG matrix B (that is in general densely populated), but only a small submatrix of it composed by a randomized selection of its rows. This is possible thanks to the choice of the trial and test

functions (localized in space and frequency, respectively) and to the previously mentioned uncertainty principle [17].

To begin with, we draw $m \ll N_{\text{dof}}$ test indices $\tau_1, \dots, \tau_m \in [N_{\text{test}}]$ i.i.d. at random according to a suitable discrete probability distribution $\boldsymbol{\pi} \in \mathbb{R}^{N_{\text{test}}}$ over $[N_{\text{test}}]$, i.e.

$$\mathbb{P}\{\tau_i = q\} = \pi_q, \quad \forall q \in [N_{\text{test}}], \forall i \in [m].$$

Next, we consider the $m \times N_{\text{dict}}$ COSSIGA discretization

$$A\mathbf{z} = \mathbf{b}, \tag{18}$$

where

$$A_{ij} := a(\psi_j, \varphi_{\tau_i}), \quad b_i := \int_{\Omega} f \varphi_{\tau_i}, \quad \forall j \in [N_{\text{dict}}], \forall i \in [m]. \tag{19}$$

The COSSIGA solution is then found by using OMP in order to compute an approximate solution $\tilde{\mathbf{x}}$ to

$$\min_{\mathbf{z} \in \mathbb{R}^{N_{\text{dict}}}} \|E(A\mathbf{z} - \mathbf{b})\|_2 \text{ s.t. } \|\mathbf{z}\|_0 \leq s. \tag{20}$$

The diagonal scaling $E \in \mathbb{R}^{m \times m}$ is defined as

$$E_{ik} = \frac{\delta_{ik}}{\sqrt{m\pi_{\tau_i}}}, \quad \forall i, k \in [m], \tag{21}$$

and accounts for the effect of the nonuniform sampling and it is chosen such that $\mathbb{E}[(EA)^*(EA)] = B^*B$, where $\mathbb{E}[\cdot]$ denotes the expected value (see [25, 29]). A very important quantity in this context is the so-called subsampling rate, i.e, the ratio m/N_{dof} : a successful application of the COSSIGA method will deliver a good approximation of the true solution with a very small subsampling rate, i.e. with $m \ll N_{\text{dof}}$.

Of course, the choice of the sampling probability distribution $\boldsymbol{\pi}$ is crucial for the effectiveness of the method. Following ideas from [25, 29] and the theoretical recipe in [10], we define $\boldsymbol{\pi}$ as a normalized upper bound to the so-called local a -coherence $\boldsymbol{\mu}$ of $\Psi_{p,l_0,L}$ with respect to Φ_R , which is defined as

$$\mu_q := \max_{j \in [N_{\text{dict}}]} (a(\psi_j, \varphi_q))^2, \quad q \in [N_{\text{test}}].$$

In practice, the exact local a -coherence $\boldsymbol{\mu}$ is replaced with a suitable upper bound $\boldsymbol{\nu}$. Namely, if

$$\mu_q \leq \nu_q, \quad \forall q \in [N_{\text{test}}],$$

then, we let

$$\pi_q = \frac{\nu_q}{\|\boldsymbol{\nu}\|_1}, \quad \forall q \in [N_{\text{test}}]. \tag{22}$$

In order to estimate $\boldsymbol{\nu}$, we employ the theoretical results in [8]. In particular, we employ the following upper bound, corresponding to [8, Equation (4.27)] (simplified by observing that $\|\mathbf{r}\|_0 \leq d$):

$$\nu_{q(\mathbf{r})} = \min \left\{ \frac{2^{(3d-2)L} \|\mathbf{r}\|_2^2}{\prod_{k=1}^d r_k^4}, \frac{\|\mathbf{r}\|_2^2}{\|\mathbf{r}\|_\infty^2 \prod_{k=1}^d r_k} \right\}, \quad \forall \mathbf{r} \in [R]^d, \tag{23}$$

where $q : [R]^d \rightarrow [N_{\text{test}}]$ corresponds to the ordering on $[R]^d$ used for the test functions.

In Figure 3, we show the sampling probability $\boldsymbol{\pi} = \boldsymbol{\nu}/\|\boldsymbol{\nu}\|_1$ in the 2D case and two corresponding random samples of frequencies \mathbf{r} . The probability distribution employed selects lower frequencies with higher probability. This is in line with standard compressive sensing results, where sampling distributions concentrated on lower frequencies are known to recover multiscale coefficients of real-world signals (e.g., natural images) significantly better than the uniform distribution (see, e.g., [1, 25]).

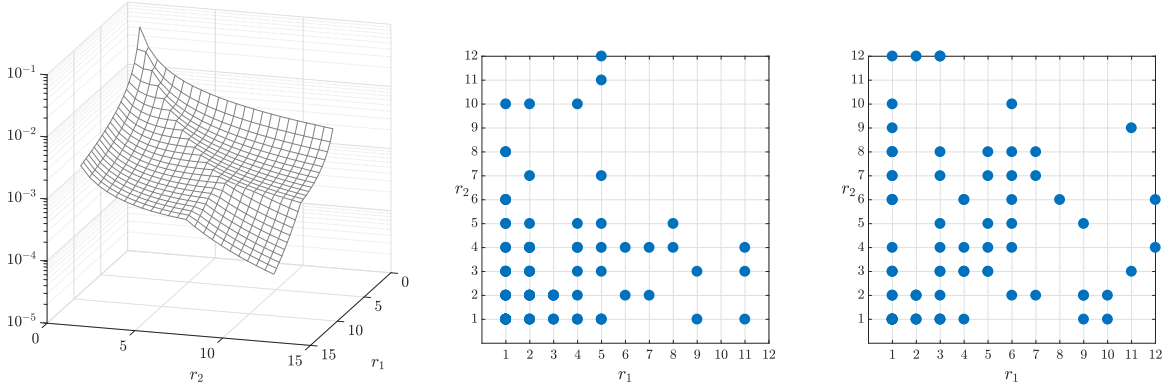


Figure 3: Left: sampling probability $\pi = \nu / \|\nu\|_1$ in the 2D case. Center and right: two sets of frequencies $\mathbf{r} = (r_1, r_2)$ randomly sampled using such sampling probability with $m = 80$. Sampling is done with replacement in order to have i.i.d. samples. The reduced test space employed in CossIGA is the span of the sine functions (10) corresponding to the selected frequencies.

Remark 2.1. *The choice of the upper bound ν made in (23) is not fully justified from the theoretical perspective, but it has to be considered heuristic. This is due to two main reasons: (i) the set of trial functions $\Psi_{p,l_0,L}$ is a dictionary and not a Riesz basis, as assumed in the theoretical framework of [8] and [10]; (ii) the estimate [8, Equation (56)] used to derive (23) holds in the case of B-spline wavelet (with $p = 1$) tested against Fourier functions defined over a periodic tensor product domain. Consequently, the influence of the degree p and the geometry of Ω are not taken into account by (23). Deriving a rigorous upper bound ν to μ for CossIGA is beyond the scope of this paper and is left to future work.*

Remark 2.2. *The convergence theory for CORSING proposed in [10] does not require ν to be a sharp upper bound to μ , but only an upper bound to μ such that $\|\nu\|_1 \ll N_{\text{dof}}$. In fact, it can be shown that when both the trial and test functions are Riesz bases, drawing m test functions with $m \geq cs\|\nu\|_1 (s \ln(eN_{\text{dof}}/s) + \ln(2s))$ (where $c > 0$ is a universal constant) using the probability distribution $\pi = \nu / \|\nu\|_1$ is sufficient to achieve a recovery error proportional to the best s -term approximation error (see [10, Theorem 3.15]). Although this theory provides sufficient conditions for sparse recovery, there are not results about the optimality of this sampling strategy.*

The CossIGA approach is summarized in Algorithm 2.1. To convince the reader of the effectiveness of the method, Figure 4 shows four different realizations of CossIGA on the problem discussed in Figure 2, obtained using a very small value of m , i.e. a very small subsampling rate. Figure 5 shows the same results, obtained using a larger value of m . As expected, increasing m improves the chances of a good recovery of the exact solution.

2.6. Practical setup for an effective use of CossIGA

Algorithm (2.1) depends on five input parameters. In analogy with classical IGA-Galerkin method, we let the user choose the B-spline degree p , the regularity of the B-splines (either $p - 1$ or 0) and the maximum hierarchical level L (or, equivalently, the mesh size $h = 2^{-L}$). Therefore, we are left with identifying two more parameters, i.e., the target sparsity s and the number of random test functions m . Of course, in an ideal setting one would have at disposal some *a priori* estimates that give an indication on the optimal choices of s and m . In this paper, these choices will instead be made numerically, based on a calibration procedure. We leave the *a priori* analysis for future work. Let us explain the philosophy behind the numerical calibration, leaving the technical details to the next section.

We assume that for given values of p and L , a good portion of the full accuracy (say, e.g., no more than twice the best approximation error of u in the B-spline space $S_p^{\text{int}}(\Xi_L, \Omega)$) can be reached using

Algorithm 2.1 CossIGA (COmpreSSive IsoGeometric Analysis)

Inputs:

- p : B-spline degree.
- reg : the regularity of the B-splines;
- L : maximum hierarchical level;
- s : target sparsity level;
- m : number of random test functions.

Procedure: $\tilde{u} = \text{CossIGA}(p, \text{reg}, L, s, m)$

1. Let R as in (16) and $N_{\text{test}} = R^d$.
2. Randomly draw $\tau_1, \dots, \tau_m \in [N_{\text{test}}]$ i.i.d. according to $\boldsymbol{\pi}$, defined as in (22)-(23).
3. Build $A \in \mathbb{R}^{m \times N_{\text{dict}}}$, $y \in \mathbb{R}^m$, and $E \in \mathbb{R}^{m \times m}$ defined as in (19) and (21).
4. Compute $\tilde{\boldsymbol{x}} \in \mathbb{R}^{N_{\text{dict}}}$ by applying s iterations of OMP to (20).
5. Let $\tilde{u} = \sum_{j=1}^{N_{\text{dict}}} \tilde{x}_j \psi_j$.

Output:

- \tilde{u} : s -sparse approximation of the solution u to (1).
-

a certain sparsity value $s^*(p, L)$, which we assume to linearly depend on N_{dof} , i.e.

$$s^*(p, L) = C(p)N_{\text{dof}}, \quad (24)$$

where $N_{\text{dof}} = N_{\text{dof}}(p, L)$ is defined as in (7). More generally, one might conjecture a nonlinear dependence between $s^*(p, L)$ and N_{dof} , of the form $s^*(p, L) = C(p)N_{\text{dof}}^{\alpha(p)}$ for some $\alpha(p) > 0$. We choose $\alpha(p) = 1$ for the sake of simplicity. Of course, we expect $s^*(p, L)$ and $C(p)$ to depend heavily on the specific solution and, in particular, on its compressibility with respect to the dictionary $\Psi_{p, l_0, L}$.

Furthermore, for each value of s we need to identify the minimum value of m such that CossIGA reaches a good portion of the accuracy corresponding to the best s -term approximation error of the solution with respect to the dictionary $\Psi_{p, l_0, L}$, defined as in (9). In principle, this m might also depend on L and p . Hence, we assume a dependence of the form

$$m(p, L, s) = D(p, L)s. \quad (25)$$

The constant D measures the compression capabilities of CossIGA and, contrary to the previous constant C , we expect a mild dependence of D on the exact solution. According to the compressive sensing theory [19], a sufficient condition to recover s -sparse vectors in \mathbb{R}^N is $m \geq c s \text{polylog}(N)$, where $c > 0$ is a universal constant and $\text{polylog}(N)$ is a polylogarithmic factor depending on the particular sampling scheme employed. These two factors are implicitly included in the constant $D(p, L)$ in (25). Moreover, the constant $D(p, L)$ depends on the bilinear form associated with the PDE considered (see [10]). For this parameter setting, the resulting subsampling rate of the CossIGA method is

$$\frac{m(p, L, s^*(p, L))}{N_{\text{dof}}} = C(p)D(p, L). \quad (26)$$

Therefore, successful compression is achieved when $C(p)D(p, L) \ll 1$.

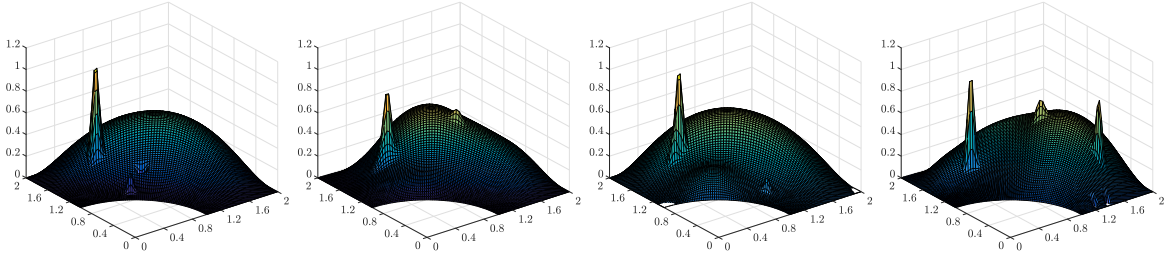


Figure 4: Four different realizations of COSSIGA for the problem of Figure 2, with $m = 76$. The subsampling rate is $m/N_{\text{dof}} = 76/1024 = 7.4\%$.

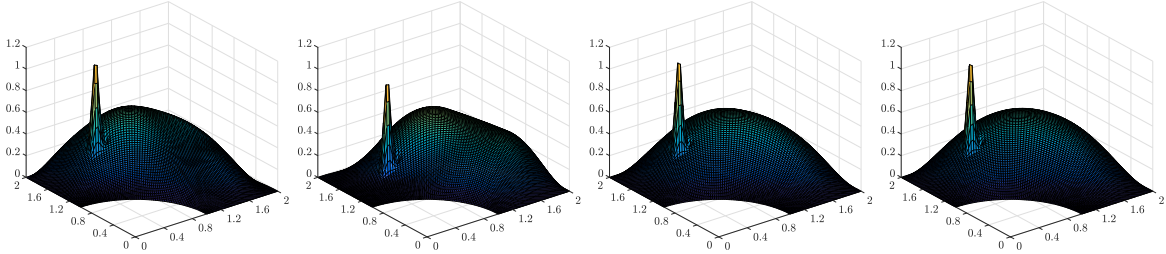


Figure 5: Four different realizations of COSSIGA for the problem of Figure 2, with $m = 304$. The subsampling rate is $m/N_{\text{dof}} = 304/1024 = 29.7\%$.

As already mentioned, determining *a priori* the constants $C(p)$ and $D(p, L)$ deserves a careful theoretical investigation and exceeds the scope of this paper. We will infer them from numerical experiments as discussed in the next section.

3. Numerical tests

In the following, we test the performance of COSSIGA for the numerical solution of (1) and for four test cases.

Case study I (Gauss 2D). As a first physical domain, we consider the quarter of ring

$$\Omega_{\text{ring}} = \{(x_1, x_2) : 1 \leq x_1^2 + x_2^2 \leq 4, x_1 \geq 0, x_2 \geq 0\}.$$

In order to study the recovery error of the method, we choose an analytical solution to (1) defined over Ω_{ring} . We call this case study ‘‘Gauss’’, corresponding to the exact solution

$$u_{\text{Gauss}}(x_1, x_2) = \exp\left(-\frac{(x_1 - 0.5)^2 + (x_2 - 1.4)^2}{(0.08)^2}\right). \quad (27)$$

The function u_{Gauss} is very close to zero on most part of the domain and has a local feature around $(0.5, 1.4)$ (see Figure 6 (left)). Although u_{Gauss} is not mathematically zero at the boundary, the homogeneous boundary conditions are satisfied within the machine precision accuracy range. In this case, the solution is expected to be sparse thanks to its small support in the physical domain. We use this first case study also to detail the calibration procedure proposed to estimate the constants C and D in (24) and (25) respectively. We then study the error of the COSSIGA solution as a function of L and for fixed p , when s and m are chosen according to (24) and (25) and using the values of C and D obtained via calibration. The accuracy achieved by COSSIGA is compared with the accuracy of the full solution of the PG system and with the accuracy of the solution obtained by using OMP to approximate the solution to (12) with s^* coefficients, where s^* is again chosen as in Equation (24).

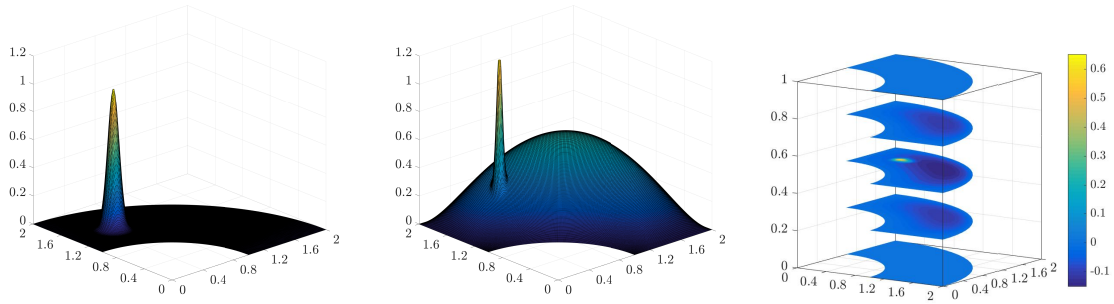


Figure 6: Exact solution u_{Gauss} (left), $u_{\text{polyGauss}}$ (center) and $u_{\text{polyGauss 3D}}$ defined by (27), (28), and (29) respectively, over the two-dimensional quarter of annulus Ω_{ring} and the three-dimensional $\Omega_{\text{thick ring}}$.

Case study II (polyGauss 2D). The second test case is called “polyGauss” and corresponds to the exact solution

$$u_{\text{polyGauss}}(x_1, x_2) = \frac{1}{5}x_1x_2(x_1^2 + x_2^2 - 1)(4 - x_1^2 - x_2^2) + \exp\left(-\frac{(x_1 - 0.5)^2 + (x_2 - 1.4)^2}{(0.04)^2}\right). \quad (28)$$

In this case, the solution has a global support and a local feature and exhibits a multiscale behaviour (see Figure 6 (center)). We use this test to investigate the sensitivity of COSSIGA with respect to the parameters C and D in Section 3.2. We achieve this goal by comparing the convergence results obtained using the constants C and D calibrated on u_{Gauss} with the results of the same test performed after recalibrating C and D on $u_{\text{polyGauss}}$.

Case study III (C^0 vs. C^{p-1} splines 2D). In the third test case, we consider again the solution $u_{\text{polyGauss}}$ and investigate the impact of the smoothness of the spline dictionary considered, i.e., whether it is advantageous to use C^0 splines instead of C^{p-1} splines as in the first two test cases (see Section 3.3).

Case study IV (polyGauss 3D). Finally, in the fourth test case we consider the three-dimensional generalization of the polyGauss test case, i.e., we let

$$\begin{aligned} \Omega_{\text{thick ring}} &= \{(x_1, x_2, x_3) : 1 \leq x_1^2 + x_2^2 \leq 4, x_1 \geq 0, x_2 \geq 0, 0 \leq x_3 \leq 1\}, \\ u_{\text{polyGauss 3D}}(x_1, x_2, x_3) &= \frac{1}{5}x_1x_2x_3(x_1^2 + x_2^2 - 1)(4 - x_1^2 - x_2^2)(x_3 - 1) \\ &\quad + \exp\left(-\frac{(x_1 - 0.5)^2 + (x_2 - 1.4)^2 + (x_3 - 0.5)^2}{(0.04)^2}\right), \end{aligned} \quad (29)$$

which is again zero within machine precision on the boundary of $\Omega_{\text{thick ring}}$. This function is displayed in Figure 6 (right). For this problem, we perform the same test as in the first case study, i.e. we compare the different methods in terms of accuracy when L varies.

3.1. Case study I: Gauss 2D

In this test, we consider B-splines of maximal regularity C^{p-1} . We will use the following terminology when referring to different approximate solutions to (1):

PG-OMP(s): Solution computed applying s iterations of OMP to the PG system (12), i.e., to compute s coefficients that approximately solve the minimization problem (17). The corresponding approximation is denoted as $\tilde{u}_{\text{PG-OMP}(s)}$. The error associated with $\tilde{u}_{\text{PG-OMP}(s)}$ is the best accuracy that we can expect from COSSIGA (p, L, s, m). In particular, in this approach there is no random compression of the test space, hence the recovery error is only due to the PG approximation and to the s -sparse approximation computed via OMP. Note also that $\|\tilde{u}_{\text{PG-OMP}(s)} - u\|_{H^1(\Omega)}$

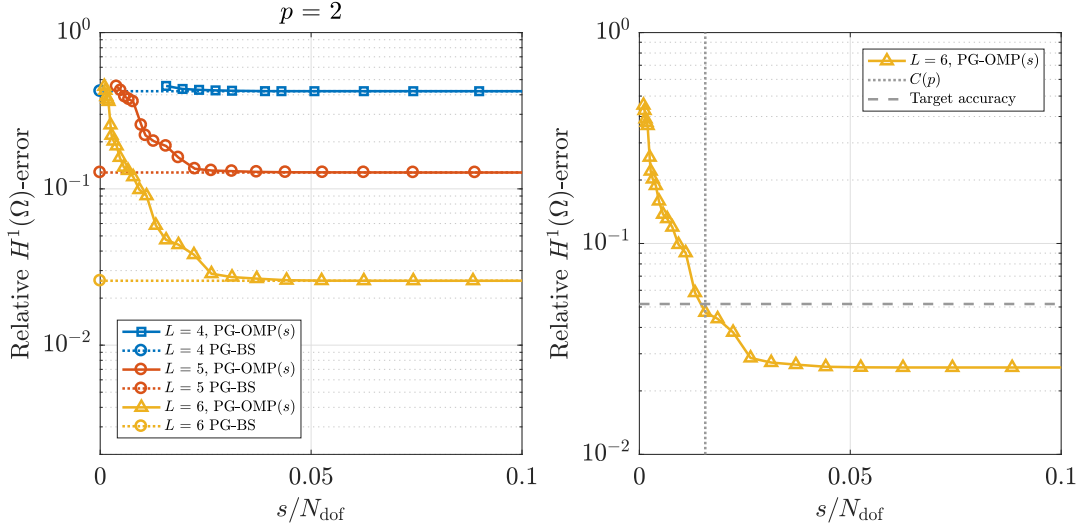


Figure 7: Case study I (Gauss 2D). Left: error of $u_{\text{OMP}(h,p,s)}$ with respect to u as a function of s , for increasing mesh refinement $L = 4, 5, 6$ and degree $p = 2$. Right: result of the C -calibration process for $L = 6$.

is an upper bound to the best s -term approximation error of u with respect to the dictionary $\Psi_{p,l_0,L}$ (defined in (9)) and can be thought as a proxy for it.

PG-BS: Least-squares solution to the PG system $Bz = c$, defined in (13). The corresponding approximation is denoted as $\tilde{u}_{\text{PG-BS}}$. Note that here the error of the solution is only due to the PG approximation, since we are neither compressing the test space nor sparsifying the solution. In particular, we expect the accuracy of PG-BS to be the best possible accuracy achievable by PG-OMP(s) for any s since $s \leq N_{\text{dict}}$.

We also performed numerical tests with a standard IGA Galerkin discretization on the finest hierarchical level, and the error obtained with this approach is almost identical to the one obtained using PG-BS. This suggests that the empirical choice (16) is sufficient to achieve the discrete inf-sup stability condition (14). Since also the number of degrees of freedom of the IGA discretization is comparable to the size of the full dictionary we use for PG-BS, only the results of the latter approach are shown in the following. We begin the discussion of this test case by detailing the procedure to estimate the constants C and D .

3.1.1. C -calibration test

For sake of explanation, we fix $p = 2$ (we have tested also $p = 1, 4$ obtaining analogous results, not shown for brevity). In Figure 7 (left), we show the relative $H^1(\Omega)$ -error computed with PG-OMP(s) for increasing values of s (normalized as s/N_{dof}), which, as already discussed, is a proxy (upper bound) to the best s -term approximation error of u with respect to the dictionary $\Psi_{p,l_0,L}$. We observe that PG-OMP(s) quickly reaches a plateau for every choice of L , at the level of the PG-BS error. This means that the same accuracy of PG-BS (or standard IGA Galerkin, as mentioned above) can be reached by activating only a small portion of the available coefficients in the dictionary, i.e., the function u_{Gauss} is compressible in $\Psi_{p,l_0,L}$, as claimed before. For a fixed accuracy, increasing the level L leads to a reduction in the sparsity percentage needed to reach such target accuracy. However, the approximation is globally less sparse for large values of L , i.e. it takes a larger percentage of dofs to reach the accuracy plateau. This means, in particular, that our assumption in Equation (24) only holds approximately (it would hold exactly if the “elbows” of the three convergence lines occurred at the same abscissa). Yet, in order to keep the complexity of our numerical illustration moderate, we do not want to complicate the model (24) and we choose a conservative value for $C(p)$ (i.e., the one for the largest value of L tested).

p	1	2	4
$C(p)$	$8.0 \cdot 10^{-3}$	$1.6 \cdot 10^{-2}$	$3.5 \cdot 10^{-2}$

Table 1: Case study I (Gauss 2D). Numerical estimate of $C(p)$ computed via the C -calibration test.

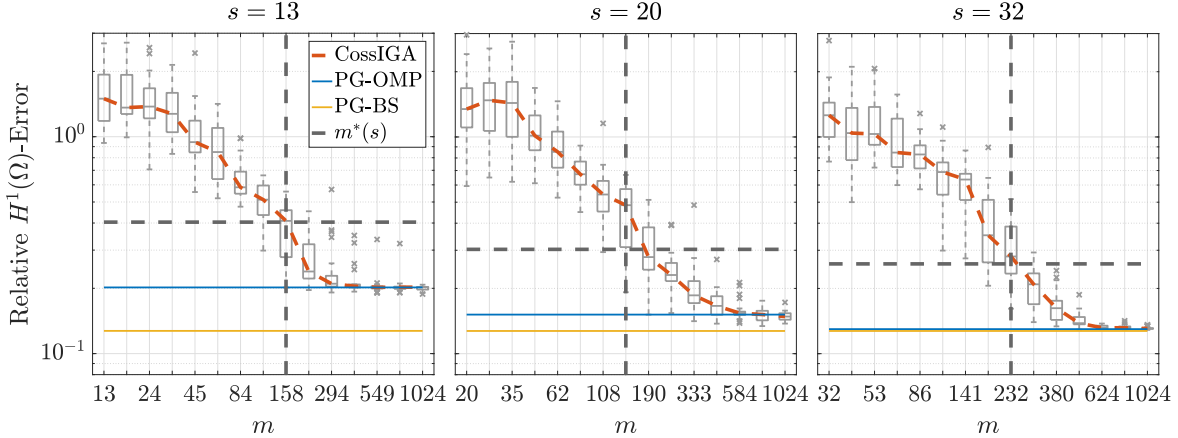


Figure 8: Case study I (Gauss 2D). D -calibration test for $p = 2$ and $L = 5$; we show error vs. m for different values of s .

Let us now illustrate in detail how to perform the C -calibration test (see Figure 7 (right)). Our goal is to choose a suitable sparsity level $s^* = s^*(p, L)$ such that the relative error achieved via PG-OMP(s^*) is comparable with the relative error of PG-BS, i.e., $\|u - \tilde{u}_{\text{OMP}(s^*)}\|_{H^1(\Omega)} \approx \mu \cdot \|u - \tilde{u}_{\text{BS}}\|_{H^1(\Omega)}$, where μ is a small constant larger than 1; in particular, we choose $\mu = 2$. We then look for the value of s among those tested that renders the error $\|u - \tilde{u}_{\text{OMP}(s)}\|_{H^1(\Omega)}$ as close as possible to $\mu \cdot \|u - \tilde{u}_{\text{BS}}\|_{H^1(\Omega)}$. More precisely, we numerically compute $s^*(p, L)$ as

$$s^*(p, L) = \arg \min_{s \in S_{\text{tested}}} \left| \|u - \tilde{u}_{\text{OMP}(s)}\|_{H^1(\Omega)} - \mu \cdot \|u - \tilde{u}_{\text{BS}}\|_{H^1(\Omega)} \right|, \quad S_{\text{tested}} = \lceil 2^{[2:0.25:11]} \rceil, \quad \mu = 2, \quad (30)$$

where we used Matlab notation to define S_{tested} . Once $s^*(p, L)$ is computed, one simply has $C(p) = s^*(p, L)/N_{\text{dof}}$. The C -calibration process is repeated for multiple values of p , leading to the values of $C(p)$ given in Table 1. In Figure 7 (right), the value of $C(p)$ with $p = 2$ (corresponding to the ratio s^*/N_{dof}) is marked with a vertical dashed line and the target accuracy

$$\mu \cdot \frac{\|u - \tilde{u}_{\text{BS}}\|_{H^1(\Omega)}}{\|u\|_{H^1(\Omega)}}, \quad \mu = 2, \quad (31)$$

with a horizontal dashed line. We note that $C(p)$ is monotonically increasing with respect to p .

3.1.2. D -calibration test

This experiment aims at estimating the constant $D(p, L)$ in Equation (25). We fix the degree p and the maximum hierarchical level L ; in particular, similarly to the previous experiments, we consider $p = 1, 2, 4$ and $L = 4, 5, 6$. For each combination of the parameters L and p we further consider different values of s , with $2 \leq s \leq s^*(p, L)$, $s^*(p, L)$ obtained via (24), where $C(p)$ estimated by the C -calibration procedure just detailed. For each value of s , we then let m vary in the interval $s \leq m \leq N_{\text{dof}}$ and we perform $n_{\text{runs}} = 25$ random runs of COSSIGA for each combination of p , L , s , and m . In particular, we let $m \geq s$ because sampling less than $m = s$ rows does not allow to compute an s -sparse approximation via OMP and we choose $m \leq N_{\text{dof}}$ because we want to achieve compression.

We plot the CossIGA relative $H^1(\Omega)$ -error as a function of m for $s = 13, 20, 32$ and $L = 5$ in Figure 8. The variability among the n_{runs} runs for each value of s and m is illustrated by using so-called box plots, which are classical tools used in statistics to represent the variability of an ensemble of

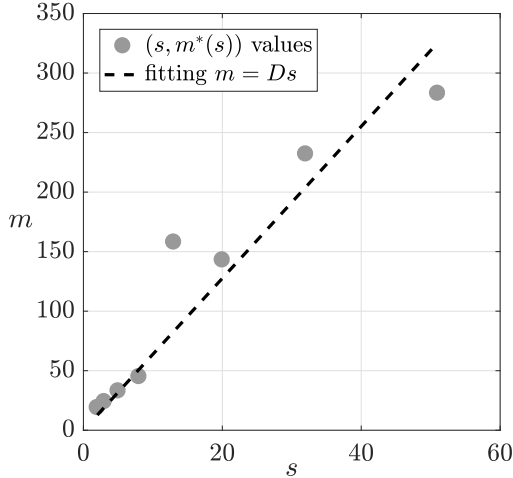


Figure 9: Case study I (Gauss 2D). D -calibration test for $p = 2$, $L = 5$.

$L \setminus p$	1	2	4
4	1.34	3.19	3.33
5	5.31	6.38	7.29
6	5.54	6.42	11.6

Table 2: Case study I (Gauss 2D). Numerical estimate of $D(p, L)$ obtained via D -calibration.

$L \setminus p$	1	2	4
4	1.07%	5.1%	11.7%
5	4.25%	10.2%	25.5%
6	4.43%	10.3%	40.6%

Table 3: Case study I (Gauss 2D). subsampling rate m/N_{dof} for different values of p and L .

values. More specifically, the rectangle extends from the 25-th to the 75-th percentile of the computed n_{runs} values; the median (50-th percentile) is marked by a horizontal line inside the rectangle; whiskers (horizontal ticks connected to the rectangle by a line) mark the smallest and largest value out of the n_{runs} values that are considered not to be outliers (in our case, the whiskers mark the 2.7-th percentile and 99.3-th percentiles), and values exceeding these bounds are marked by “cross” markers. In each plot, we add lines connecting the median values of the box plots to ease the visualization of the convergence of COSSIGA, and horizontal lines that mark the accuracy obtained by PG-OMP(s) and PG-BS. We can make several observations:

- As m increases, the accuracy of COSSIGA eventually reaches the accuracy of PG-OMP(s). Note that when the convergence curve of COSSIGA approaches this bound, it exhibits an “elbow”, marking the point where the decay of the error with respect to m slows significantly.
- As s increases (plots from left to right), the PG-OMP(s) solution error decreases (as predicted already by Figure 7), and reaches the PG-BS accuracy for s large enough ($s = 32$ in Figure 8).
- As we increase s , we need a larger m to reach full accuracy.

Now, let us explain how to perform D -calibration given the data computed in the setting above. For every value of s , we select the value of m closest to the elbow of the convergence curve (up to a prescribed relative tolerance) similarly to the case of C -calibration. In particular, we choose

$$m^*(s) = \arg \min_{s \leq m \leq N_{\text{dof}}} \left| \|u - \tilde{u}_{\text{COSSIGA}(s,m)}\|_{H^1(\Omega)} - \mu \cdot \|u - \tilde{u}_{\text{OMP}(s)}\|_{H^1(\Omega)} \right|, \quad \mu = 2. \quad (32)$$

With this choice, $\|u - \tilde{u}_{\text{COSSIGA}(s,m^*(s))}\|_{H^1(\Omega)} \approx 2\|u - \tilde{u}_{\text{OMP}(s)}\|_{H^1(\Omega)}$. Recalling (25), we can now find $D(p, L)$ by computing the best curve of the form $m = Ds$ fitting in the least-squares sense the data $(s, m^*(s))$ for the considered values of s . Note that we are deliberately not considering the zero-order term in the equation, i.e., we are not fitting an affine model $m = Ds + m_0$, since we are looking for a linear law of the form (25). Figure 9 illustrates this process. The resulting values of $D(p, L)$ are listed in Table 2. As expected, D increases overall with L and p .

3.1.3. Convergence test

We are now in a position to study the convergence of COSSIGA with respect to the hierarchical level L (or, equivalently, to the mesh size $h = 2^{-L}$) for fixed p . We consider different values of $L = 4, 5, 6$

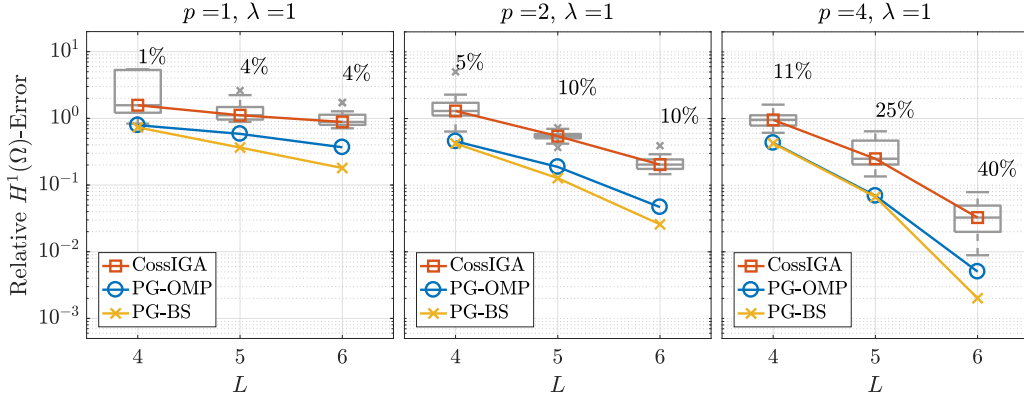


Figure 10: Case study I (Gauss 2D). Convergence analysis of CossIGA for the “Gauss” case study for $p = 1, 2, 4$ (left to right). The percentage above each box is the subsampling rate m/N_{dof} .

and we study the recovery error as a function of the hierarchical level L . For each value of L and p (we recall that in this test we consider B-splines of maximal regularity C^{p-1}), we consider a the following CossIGA approximation (see Algorithm 2.1):

$$\text{CossIGA}(p, p-1, L, s^*, m^*),$$

with $s^* = C(p)N_{\text{dof}}$ and $m^* = D(p, L)s^* = D(p, L)C(p)N_{\text{dof}}$. Table 3 illustrates the subsampling rate $m/N_{\text{dof}} = C(p)D(p, L)$ (recall (26)) of CossIGA for different values of p and L , using the constants $C(p)$ and $D(p, L)$ estimated in Sections 3.1.1 and 3.1.2. In particular, with these choices we have

$$\|u - \tilde{u}_{\text{CossIGA}(s,m)}\|_{H^1(\Omega)} \approx 2\|u - \tilde{u}_{\text{OMP}(s)}\|_{H^1(\Omega)} \approx 4\|u - \tilde{u}_{\text{BS}}\|_{H^1(\Omega)},$$

i.e., we are losing a factor 4 from the best accuracy available at resolution h . All the values in Table 3 are below 100%, hence corresponding to a successful subsampling.

Given that most of the values in Table 3 are significantly smaller than 100%, in the convergence test we also investigate the effects of taking the constants C and D larger than prescribed by the calibration tests, i.e., multiplying both C and D by a factor $\lambda \geq 1$: a choice of λ strictly greater than 1 is expected to decrease the compression but improve the accuracy and robustness of CossIGA. We also set a upper threshold, so that an minimal compression is always enforced. Specifically, we set

$$m/N_{\text{dof}} = \min\{\lambda^2 C(p)D(p, L), 80\%\}.$$

We repeat again $n_{\text{runs}} = 25$ tests of CossIGA for each value of L using the above recipe.

Results are reported in Figure 10 in terms of relative $H^1(\Omega)$ -error vs. L . We show the n_{runs} values using box plots, and we add convergence curves for the PG-BS solution and the PG-OMP(s) solution with $s = s^*(p, L)$. This Figure shows results for increasing p and $\lambda = 1$ (i.e., using C and D as calibrated). We first note that, as expected, PG-OMP(s) converges at a lower rate than PG-BS. The convergence of CossIGA has an even lower rate, but the loss of accuracy of CossIGA with respect to PG-OMP(s) is moderate, especially for lower degrees $p = 1, 2$, and considered the quite small subsampling rates imposed (reported in the plots with numbers above each box).

Convergence with respect to L , shown in Figure 10, is not really a representative quantity for the computation cost of CossIGA. We therefore also compare the methods by plotting the relative $H^1(\Omega)$ -error as a function of the number of computed coefficients, defined by

$$N_{\text{comp}} := \begin{cases} s, & \text{for PG-OMP}(s) \text{ and CossIGA,} \\ N_{\text{dict}}, & \text{for PG-BS.} \end{cases} \quad (33)$$

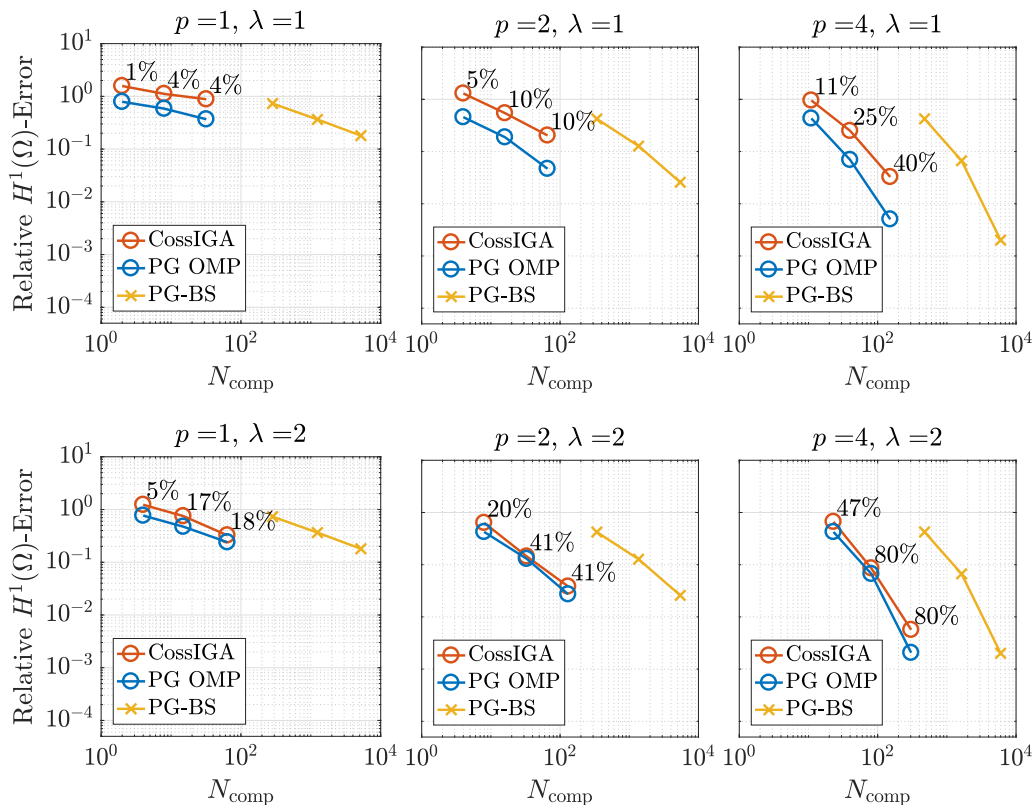


Figure 11: Case study I (Gauss 2D). Convergence analysis of CossIGA for the “Gauss” case study. In this figure we report error versus number of degrees of freedom. Top line: results for $p = 1, 2, 4$ and $\lambda = 1$ (left to right). Bottom line: same thing with $\lambda = 2$. The percentage above each marker is the subsampling rate m/N_{dof} .

This quantity is also not entirely representative of the actual computational cost. It rather represents the optimal cost that can be achieved with ideal algorithms and implementation (for comparison, the class of sublinear-time algorithms known as “sparse Fourier transforms” are able to recover an s -sparse signal of \mathbb{R}^N with $O(s \text{ polylog}(N))$ flops from compressive Fourier measurements [20]). Results are reported in Figure 11 and show the rather significant improvement in convergence that could be potentially reached with a careful implementation of CossIGA. In this Figure (and in most of the remaining ones of this paper), we show only the median convergence of CossIGA instead of the box plots. In detail, the top half shows the results with $\lambda = 1$, while the bottom one show results for $\lambda = 2$. As expected, the effect of setting $\lambda = 2$ are: (i) PG-OMP is closer to PG-BS (since the number s of coefficients of the solution that we are computing is doubled) (ii) CossIGA is closer to PG-OMP (since we are doubling the number of rows that we sample from the PG matrix) (iii) the subsampling rate is four times larger, and in particular for $p = 4$ and large L the threshold of 80% is enforced.

3.2. Case study II: polyGauss 2D

In this second test, we consider the Poisson problem with exact solution $u_{\text{polyGauss}}$ defined in (28). This solution has a clear multilevel structure since it is composed of a “coarse component” (the polynomial in (28)) and a “fine detail” (the Gaussian peak), while the coarse component was missing in the previous test. In this test, as in the previous one, we consider B-splines of maximal regularity C^{p-1} .

We take advantage of this test also to verify the robustness of the method with respect to the calibration of the constants C and D , which is an expensive procedure (that one would rather do a limited number of times in advance, if not once – or possibly skip altogether if theoretical estimates

p	1	2	4
$C(p)$	$4.0 \cdot 10^{-3}$	$4.6 \cdot 10^{-3}$	$1.0 \cdot 10^{-2}$

Table 4: Case study II (polyGauss 2D). Numerical estimate of $C(p)$ computed via the C -calibration test for the function $u_{\text{polyGauss}}$.

$L \setminus p$	1	2	4
4	1.80	1.00	1.00
5	1.76	4.24	4.64
6	4.48	11.45	17.77

Table 5: Case study II (polyGauss 2D). Numerical estimate of $D(p, L)$ obtained via D -calibration for the polyGauss test.

of C and D were available). The results for the new calibrations are reported in Tables 4 and 5 for C and D , respectively, and they should be compared with the corresponding Tables 1 and 2 obtained for the Gauss test case.

This comparison shows that the constant C changes slightly (order of magnitude are identical though), as expected. In particular, the values of C for the polyGauss test are smaller than for Gauss, which means that $u_{\text{polyGauss}}$ is more compressible than u_{Gauss} . Perhaps more surprising (and against our assumptions) is that also the constants D change, albeit being again in the same range of magnitude. There is however no clear trend, i.e., sometimes the D associated with the Gauss test is larger than the D associated with the polyGauss test, and vice versa. We emphasize, however, that the calibration is a numerical procedure that can be sensitive to many tuning parameters (e.g., choice of the values of s, m , number of runs per test n_{runs} , tolerance factors, sampling probability distribution π for the test functions). Consequently, a conclusive statement on whether the value of D is independent of the solution u or not is hard to make and is postponed to further and deeper analyses.

We compare the convergence plots when both C and D uncalibrated (i.e., using the constants for the Gauss test in the polyGauss one) and calibrated for this test, with the aim of studying the sensitivity of COSSIGA with respect to the choice of these parameters. The results are reported in Figures 12 and 13. The former shows results for $p = 1, 2, 4$ and $\lambda = 1$ for uncalibrated C, D and the latter compares the results with calibrated and uncalibrated C, D for selected values of p and λ . Figure 12 shows that COSSIGA is more effective than in the Gauss test since the convergence of COSSIGA is closer to the convergence of PG-OMP, and the error reached by PG-OMP is closer to the error reached by PG-BS than in the previous test (cf. Figure 11). This is due to the higher compressibility of the solution at hand: since we “froze” the subsampling rate but the solution considered in this test is more compressible, PG-OMP gets closer in error to PG-BS for the given number of coefficients s , and COSSIGA gets closer to PG-OMP for the given number of sampled rows.

In Figure 13 we compare the results of the calibrated and uncalibrated procedure for $p = 4$ (other values of p give similar results). We see that in the calibrated case, the convergence of PG-OMP is actually further from the PG-BS results, which is to be expected since C is substantially smaller after recalibration, so less terms are computed; and similarly, the convergence of COSSIGA is further from PG-OMP because less rows are now computed. In other words, as one would expect, the results obtained with the uncalibrated constants are (in this case) suboptimal, in the sense that the same target accuracy relative to PG-BS can be obtained with a smaller subsampling rate (i.e., with smaller values of C and D).

3.3. Case study III: C^0 vs. C^{p-1} splines 2D

In this test, we assess the performance of COSSIGA when C^0 splines are employed instead of $C^{(p-1)}$ splines, motivated by the fact that C^0 splines are supported on one or two elements only (instead of $p+1$ elements as in the case of $C^{(p-1)}$ splines), which might further promote sparsity of solutions with localized features. On the other hand, it is well-known that $C^{(p-1)}$ splines yield a better accuracy per degree of freedom, see e.g. [5], so it is not clear *a priori* what choice should be more favorable in terms of error-dof ratio. We limit ourselves to the polyGauss test and recalibrate once more C, D for this test.

In Figure 14, we show the results obtained with $p = 4, \lambda = 1$. In the case of C^0 splines we consider $L = 4, 5, 6$ and represent the results with full lines, while in the case of $C^{(p-1)}$ splines we consider $L = 3, 4, 5$ and represent the results with dashed lines. The use of different discretization levels for the

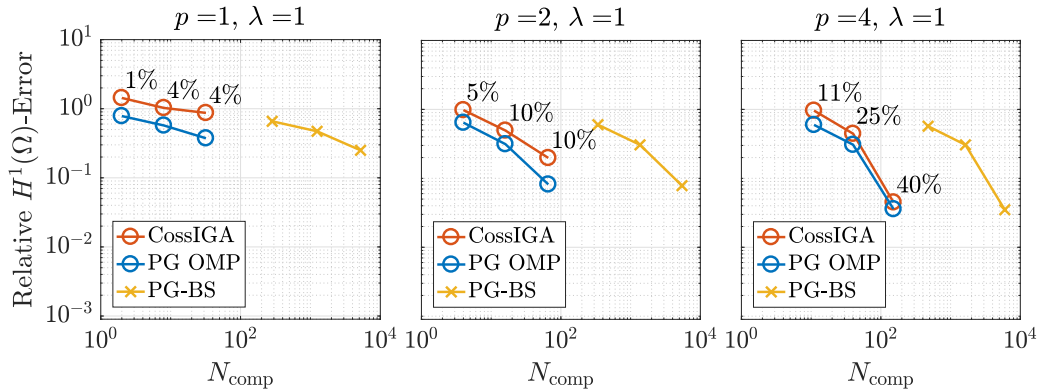


Figure 12: Case study II (polyGauss 2D). Convergence analysis of CossIGA for the polyGauss case study without performing C -calibration on $u_{\text{polyGauss}}$. The percentage above each marker is the subsampling rate m/N_{dof} .

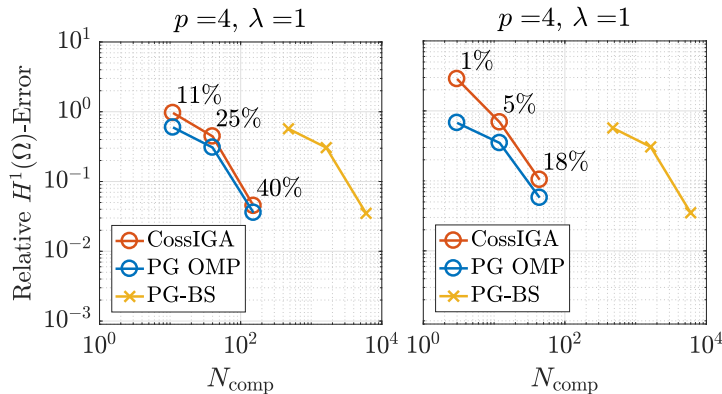


Figure 13: Case study II (polyGauss 2D). Convergence analysis of CossIGA for the polyGauss case study with C -calibration on $u_{\text{polyGauss}}$. Here we fix $p = 4$ and we compare the following convergence plots. Left: uncalibrated $C, D, \lambda = 1$ (this plot is also in Figure 12); Right: calibrated $C, D, \lambda = 1$. The percentage above each marker is the subsampling rate m/N_{dof} .

two approaches allows to make a better comparison. Indeed, as can be seen in the plot, in this case the error we obtain with PG-BS and PG-OMP using C^{p-1} splines for a given discretization level is almost identical to the error obtained using C^0 splines for the following discretization level.

The C^{p-1} approach, however, yields a lower number of degrees of freedom, showing an advantage over the C^0 case. This is assessed by the distance between the PG-BS lines, and a similar distance (possibly a bit larger) can be observed between the PG-OMP lines is approximately the same. The advantage of C^{p-1} splines is then of course inherited by the CossIGA results. This suggests that the better error-dof ratio yielded by high regularity holds also in the context of compressed sensing.

3.4. Case study IV: polyGauss 3D

In this case study, we consider the three-dimensional version of the Poisson problem with exact solution in Equation (29). Intuitively, we expect this solution to be even sparser than the 2D equivalent since the localized feature (i.e., the exponential term in (29)) is essentially supported on the horizontal mid-plan of the domain, and is zero in most of the rest of the volume. Thus, the setup is ideal for CossIGA. In this test, we recalibrate the constants C, D and we fix $p = 2$ for simplicity. An immediate verification of the fact that the solution is much sparser and compressible than before is that now we can choose a much smaller constant μ in the calibration of both C and D , cf. Equations (30) and (32): specifically, we choose $\mu = 1.01$ instead of $\mu = 2$ for the C -calibration (which means that much fewer

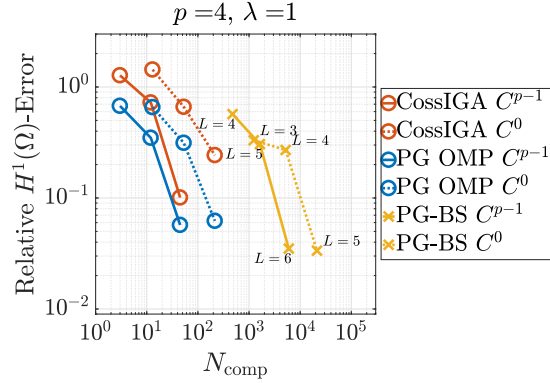


Figure 14: Case study III (C^0 vs. C^{p-1} splines 2D). Results obtained with $p = 4$, $\lambda = 1$. We use different discretization levels for the C^0 case ($L = 3, 4, 5$) and for the C^{p-1} case ($L = 4, 5, 6$).

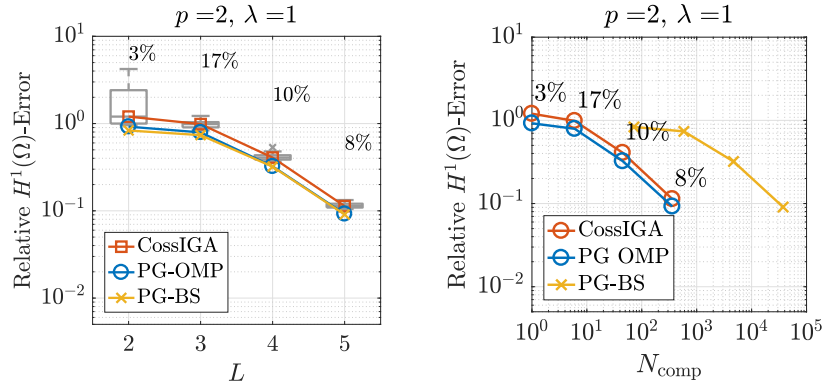


Figure 15: Case study IV (polyGauss 3D). Results for $p = 2$, $C^{(p-1)}$ splines, $\lambda = 1$. Left: error vs L ; right: error vs N_{dof} . The percentage above each box/marker is the subsampling rate m/N_{dof} .

coefficients are significantly nonzero) and $\mu = 1.2$ instead of $\mu = 2$ for the D -calibration (and, hence, that fewer rows of the matrix are needed to recover a satisfactory approximation of the solution).

Given these premises, we expect a good performance of CossIGA and indeed this is what can be deduced from the convergence plots reported in Figure 15, which shows the convergence of the error with respect to both the refinement level L and the number of computed coefficients N_{comp} , defined in Equation (33), in the left and right panel, respectively. The boxes in the left panel are very thin. This means that the variability due to randomness is almost negligible. Moreover, in the left panel the CossIGA median convergence is very close to the one of PG-BS. This can be explained by the smaller values of μ used in the C - and D -calibration procedures. In the right panel we see that we can essentially recover the accuracy of the full PG-BS solution with two orders of magnitude less degrees of freedom and an overall subsampling rate smaller than 20%.

4. Conclusions

We have shown that the compressive sensing paradigm can be successfully applied to solve PDEs on domains with a nontrivial geometry, and that the sparsity principle can be leveraged to discretize PDEs by means of a compressive Petrov-Galerkin discretization, leading to the CossIGA (COMPRESSive IsoGeometric Analysis) method. This paper is essentially a proof of concept. Its aim is to show that the proposed method can be an attractive alternative to speed up IGA solvers whenever the solution can be expressed over a basis (or, possibly, a dictionary) that enhances its sparsity.

From a theoretical perspective, many issues remain open, such as estimating the local a -coherence and providing effective *a priori* estimates for the constants C and D , which are two of the cornerstones to make the method effective. These issues should be addressed in order to prove a formal convergence theorem for COSSIGA, which hence seems far from being a trivial task.

Concerning the computational efficiency, we remark that our Matlab implementation of COSSIGA is not optimized yet. As a consequence, the different algorithms considered in this paper were compared only in terms of number of computed coefficients, and not in terms of computation time. Devising and effective implementation of COSSIGA is a key open issue.

Finally, the connections between the COSSIGA approach and the standard local adaptivity algorithms for IGA deserve further investigations.

5. Acknowledgements

SB acknowledges the PIMS Postdoctoral Training Centre in Stochastics, NSERC through grant R611675, and the Faculty of Arts and Science of Concordia University for the financial support. The authors thank Ben Adcock for fruitful discussions about COSSIGA and for supporting LT's visits at SFU in 2018 and 2019, partially funded by the PIMS CRG in "High-dimensional Data Analysis". The authors also thank Fabio Nobile and John Evans for their feedback on an earlier version of this manuscript. LT and MT also received support from the Gruppo Nazionale Calcolo Scientifico-Istituto Nazionale di Alta Matematica "Francesco Severi" (GNCS-INDAM).

References

- [1] B. Adcock, A. C. Hansen, C. Poon, and B. Roman. Breaking the coherence barrier: A new theory for compressed sensing. In *Forum Math., Sigma*, volume 5. Cambridge University Press, 2017.
- [2] B. Adcock and D. Huybrechs. Frames and numerical approximation. *SIAM Rev.*, 61(3):443–473, 2019.
- [3] P. Antolin, A. Buffa, F. Calabro, M. Martinelli, and G. Sangalli. Efficient matrix computation for tensor-product isogeometric analysis: The use of sum factorization. *Comput. Methods Appl. Mech. Engrg.*, 285:817–828, 2015.
- [4] J. Beck, G. Sangalli, and L. Tamellini. A sparse-grid isogeometric solver. *Comput. Methods Appl. Mech. Engrg.*, 335:128–151, 2018.
- [5] L. Beirão da Veiga, A. Buffa, G. Sangalli, and R. Vázquez. Mathematical analysis of variational isogeometric methods. *Acta Numer.*, 23:157–287, 5 2014.
- [6] C. Bracco, A. Buffa, C. Giannelli, and R. Vázquez. Adaptive isogeometric methods with hierarchical splines: An overview. *Discrete Contin. Dyn. Syst. - A*, 39(1):241–261, 2019.
- [7] S. Brugiapaglia. *COmpRessed SolvING: sparse approximation of PDEs based on compressed sensing*. PhD thesis, Italy, 2016.
- [8] S. Brugiapaglia, S. Micheletti, F. Nobile, and S. Perotto. Wavelet-Fourier CORSING techniques for multi-dimensional advection-diffusion-reaction equations. *arXiv preprint arXiv:1812.09403*, 2018.
- [9] S. Brugiapaglia, S. Micheletti, and S. Perotto. Compressed solving: A numerical approximation technique for elliptic PDEs based on Compressed Sensing. *Comput. Math. Appl.*, 70(6):1306–1335, 2015.
- [10] S. Brugiapaglia, F. Nobile, S. Micheletti, and S. Perotto. A theoretical study of COmpRessed SolvING for advection-diffusion-reaction problems. *Math. Comp.*, 87(309):1–38, 2018.

- [11] F. Calabro, G. Sangalli, and M. Tani. Fast formation of isogeometric Galerkin matrices by weighted quadrature. *Comput. Methods Appl. Mech. Engrg.*, 316:606–622, 2017.
- [12] E. J. Candès, J. Romberg, and T. Tao. Robust uncertainty principles: Exact signal reconstruction from highly incomplete frequency information. *IEEE Trans. Inform. Theory*, 52(2):489–509, 2006.
- [13] N. Collier, L. Dalcin, D. Pardo, and V. M. Calo. The cost of continuity: performance of iterative solvers on isogeometric finite elements. *SIAM J. Sci. Comput.*, 35(2):A767–A784, 2013.
- [14] L. B. Da Veiga, L. F. Pavarino, S. Scacchi, O. B. Widlund, and S. Zampini. Isogeometric BDDC preconditioners with deluxe scaling. *SIAM J. Sci. Comput.*, 36(3):A1118–A1139, 2014.
- [15] M. Donatelli, C. Garoni, C. Manni, S. Serra-Capizzano, and H. Speleers. Symbol-based multigrid methods for Galerkin B-spline isogeometric analysis. *SIAM J. Numer. Anal.*, 55(1):31–62, 2017.
- [16] D. L. Donoho. Compressed sensing. *IEEE Trans. Inform. Theory*, 52(4):1289–1306, 2006.
- [17] D. L. Donoho and P. B. Stark. Uncertainty principles and signal recovery. *SIAM J. Appl. Math.*, 49(3):906–931, 1989.
- [18] Daniel Drzisga, Brendan Keith, and Barbara Wohlmuth. The surrogate matrix methodology: Low-cost assembly for isogeometric analysis. *Comput. Methods Appl. Mech. Engrg.*, 361:112776, 2020.
- [19] S. Foucart and H. Rauhut. *A mathematical introduction to compressive sensing*. Springer, 2013.
- [20] A. C. Gilbert, P. Indyk, M. Iwen, and L. Schmidt. Recent developments in the sparse Fourier transform: A compressed Fourier transform for big data. *IEEE Signal Process. Mag.*, 31(5):91–100, 2014.
- [21] C. Hofreither. A black-box low-rank approximation algorithm for fast matrix assembly in isogeometric analysis. *Comput. Methods Appl. Mech. Engrg.*, 333:311–330, 2018.
- [22] C. Hofreither, S. Takacs, and W. Zulehner. A robust multigrid method for isogeometric analysis in two dimensions using boundary correction. *Comput. Methods Appl. Mech. Engrg.*, 316:22 – 42, 2017. Special Issue on Isogeometric Analysis: Progress and Challenges.
- [23] T. J. R. Hughes, J. A. Cottrell, and Y. Bazilevs. Isogeometric analysis: CAD, finite elements, NURBS, exact geometry and mesh refinement. *Comput. Methods Appl. Mech. Engrg.*, 194(39):4135–4195, 2005.
- [24] H. Kang, M.-J. Lai, and X. Li. An economical representation of PDE solution by using compressive sensing approach. *Comput.-Aided Des.*, 115:78 – 86, 2019.
- [25] F. Kraemer and R. Ward. Stable and robust sampling strategies for compressive imaging. *IEEE Trans. Image Process.*, 23(2):612–622, 2014.
- [26] A. Mantzaflaris, B. Jüttler, B. N. Khoromskij, and U. Langer. Low rank tensor methods in Galerkin-based isogeometric analysis. *Comput. Methods Appl. Mech. Engrg.*, 316:1062–1085, 2017.
- [27] B. K. Natarajan. Sparse approximate solutions to linear systems. *SIAM J. Comput.*, 24(2):227–234, 1995.
- [28] A. Quarteroni and A. Valli. *Numerical approximation of partial differential equations*, volume 23. Springer Science & Business Media, 2008.
- [29] H. Rauhut and R. Ward. Sparse Legendre expansions via ℓ_1 -minimization. *J. Approx. Theory*, 164(5):517–533, 2012.

- [30] G. Sangalli and M. Tani. Isogeometric Preconditioners Based on Fast Solvers for the Sylvester Equation. *SIAM J. Sci. Comput.*, 38(6):A3644–A3671, 2016.
- [31] G. Sangalli and M. Tani. Matrix-free weighted quadrature for a computationally efficient isogeometric k-method. *Comput. Methods Appl. Mech. Engrg.*, 338:117–133, 2018.
- [32] R. Tielen, M. Möller, D. Göttsche, and C. Vuik. Efficient p -multigrid methods for isogeometric analysis. *arXiv preprint arXiv:1901.01685*, 2019.
- [33] R. Vazquez. A new design for the implementation of isogeometric analysis in Octave and Matlab: GeoPDEs 3.0. *Comput. Math. Appl.*, 72(3):523 – 554, 2016.